applied sciences

MDPI

Article

Divergent Kinetic Modeling of Wine Aging Across Bulk Storage and Bottle Environments

Piernicola Masella, Agnese Spadi, Ferdinando Corti *, Alessandro Parenti and Giulia Angeloni

Department of Agriculture, Food, Environment and Forestry (DAGRI), University of Florence, Piazzale Delle Cascine 18, 50144 Florence, Italy; piernicola.masella@unifi.it (P.M.); agnese.spadi@unifi.it (A.S.); alessandro.parenti@unifi.it (A.P.); giulia.angeloni@unifi.it (G.A.)

* Correspondence: ferdinando.corti@unifi.it; Tel.: +39-0552755700

Abstract

Physicochemical transformations in wine aging are strongly influenced by storage environment and scale. While kinetic modeling has been extensively applied to bulk aging systems, bottle aging is often treated as a continuation of cellar evolution despite representing a different physicochemical regime. A reaction-kinetics framework was applied to assess whether wine aging in bulk and bottle environments can be described by a unified model or instead requires divergent quantitative descriptions. A Sangiovese red wine was aged for six months under controlled conditions in inert bulk systems (stainless steel and a non-porous composite material), a porous bulk system (raw earthenware), and glass bottles. Key physicochemical parameters, including dissolved oxygen, oxidation–reduction potential, free sulfur dioxide, anthocyanins, polymerized pigments, and colorimetric indices, were monitored through non-invasive and laboratory analysis. Exploratory multivariate analysis showed that inert systems follow overlapping compositional trajectories, indicating stable chemical evolution, whereas bottle-aged wines exhibited greater variability. Kinetic analysis revealed comparable oxygen-limited behavior and buffered oxidation–reduction evolution in inert bulk systems, whilst bottle aging displayed different oxygen and sulfur dioxide dynamics, consistent with scale effects and altered oxygen partitioning. Overall, bottle aging cannot be reliably predicted by extrapolation of bulk storage kinetics and requires boundary-condition-aware descriptors accounting for scale and environmental constraints.

Keywords: wine processing; storage systems; oxidative stability; red wine aging; process kinetics; storage material

Academic Editor: Małgorzata Ziarno

Received: 12 April 2026
Revised: 7 May 2026
Accepted: 8 May 2026
Published: 13 May 2026

1. Introduction

The production of high-quality red wines is a complex sequence of biochemical and physical transformations in which the aging phase plays a role of paramount importance [1,2]. While the intrinsic potential of a wine is largely established in the vineyard and during alcoholic fermentation, it is the post-fermentation aging period—ranging from a few months to several years—that ultimately defines its sensory profile, physicochemical stability, and commercial value. During this interval, wine evolves from a chemically unstable hydroalcoholic matrix, rich in primary aromas and reactive phenolic compounds, into a more equilibrated system characterized by stabilized color and a softened mouthfeel [3]. Historically, wine aging has been managed through empirical practices, with the selection of storage vessels dictated primarily by tradition and material availability.

In modern precision enology, however, this empirical approach is increasingly inadequate. A transition toward a predictive, engineering-based framework is required—one in which the aging vessel is no longer regarded as a passive container, but as a chemical reactor whose physical and material properties define boundary conditions for reaction pathways and kinetics [4].

At the molecular level, red wine aging is governed by a complex network of oxidation, condensation, and rearrangement reactions involving the phenolic fraction, particularly anthocyanins and flavanols [3,5]. In young red wines, anthocyanins predominantly exist in labile forms that are susceptible to degradation through pH-dependent equilibria, bleaching, and nucleophilic attack. Aging promotes the gradual formation of polymeric pigments through condensation reactions between anthocyanins and tannins, leading to enhanced color stability and modified sensory perception [6,7]. These processes are strongly influenced by oxygen availability. Dissolved oxygen, often in conjunction with iron- and copper-mediated redox cycling, facilitates the formation of acetaldehyde from ethanol, which acts as a key bridging molecule in flavonoid polymerization [8–10]. The resulting increase in phenolic molecular weight contributes both to chromatic stabilization and to a reduction in perceived astringency through decreased tannin reactivity with salivary proteins [3].

Oxygen availability, in turn, is largely dictated by the physical properties of the aging environment, leading to a functional distinction between porous and non-porous bulk storage systems. Porous vessels, such as oak barrels and unglazed earthenware containers, permit a continuous but limited ingress of atmospheric oxygen (micro-oxygenation), accelerating oxidative and polymerization reactions [11,12]. These systems, however, may also introduce additional sources of variability due to the release of exogenous organic compounds or inorganic ions [13]. In contrast, non-porous vessels such as stainless steel tanks are designed to minimize gas exchange, confining wine evolution to reactions driven by residual dissolved oxygen introduced during fermentation or cellar operations [14,15]. Under these conditions, reaction rates are typically slower, favoring the preservation of primary varietal attributes [16].

Beyond differences among bulk storage systems, a major and still insufficiently addressed discontinuity in enological kinetics concerns the transition from tank aging to bottle aging. Kinetic modeling in enology has traditionally focused on large-volume systems, applying zero-, first-, or second-order rate laws to describe temporal changes in phenolic composition or color parameters [17]. The bottle phase is frequently treated as a static or poorly characterized continuation of bulk aging, despite representing a fundamentally different physicochemical system. Oxygen dynamics in bottles are unique: gas exchange occurs exclusively through the closure, at extremely low and closure-dependent rates often described as nano-oxygenation [18–20]. Once the limited oxygen initially present in the headspace and dissolved phase is consumed, bottled wine may enter a markedly reductive regime, in which alternative reaction pathways—such as slow hydrolysis reactions, molecular rearrangements, and the formation or degradation of sulfur-containing compounds—become increasingly relevant [21,22]. These conditions differ qualitatively from those prevailing in bulk storage, even under nominally inert conditions. On this basis, we propose a divergent kinetic framework, hypothesizing that the mathematical descriptions and rate constants applicable to wine aging in bulk storage systems cannot be linearly extrapolated to the bottle environment. Rather than representing a simple change in reaction rates, the transition from bulk storage to bottle aging is expected to involve a shift in dominant mechanisms and rate-limiting steps, from oxygen-controlled regimes to temperature- and matrix-controlled processes characteristic of sealed micro-reactors [23,24].

To investigate this hypothesis, the present study conducts a comparative kinetic analysis of a Sangiovese red wine aged under controlled bulk storage conditions and in glass bottles. Bulk aging was performed using both porous and non-porous vessels. In addition to conventional stainless steel tanks, a non-porous composite material was deliberately included as an independent inert benchmark. Importantly, this material is not proposed as a candidate for enological application; rather, it serves as a controlled experimental tool to test the generality and material-independence of kinetic models developed for inert bulk storage conditions.

The novelty of this study lies in explicitly testing whether kinetic descriptors derived under bulk storage conditions remain valid after transition to bottle aging, or whether storage scale imposes distinct boundary conditions requiring divergent quantitative descriptions. By monitoring key chemical and physical parameters, the study aims to assess the robustness of kinetic descriptions for bulk aging across different inert boundary conditions and to quantitatively characterize the kinetic divergence between bulk storage and bottle aging. Because the present work was conducted on a single wine matrix under controlled experimental conditions, the resulting descriptors should be interpreted as a mechanistic and methodological framework for comparing storage boundary conditions rather than as universally transferable kinetic constants.

2. Materials and Methods

2.1. Wine Matrix and Experimental Design

The experimental trial was conducted on a Sangiovese red wine (Chianti DOCG/Chianti Bio, 2022 vintage) produced by Fattoria di Petrognano (Montelupo Fiorentino, Florence, Italy). The wine originated from a single homogeneous batch sampled after completion of alcoholic and malolactic fermentations to ensure identical initial chemical composition across treatments. Wine aging was carried out for six months in an underground cellar characterized by natural thermal buffering. Four storage conditions were investigated: (i) stainless steel (SS) tanks; (ii) Corian® tanks; (iii) raw earthenware amphorae (porous bulk system); and (iv) glass bottles (0.75 L Bordeaux type), sealed with technical closures (finite-volume reference).

A strict anaerobic control was not included because the objective of the study was to compare realistic enological storage conditions rather than idealized oxygen-free systems. All investigated configurations therefore reflect practical storage boundary conditions relevant to cellar aging and bottling.

Bulk containers (Corian®, stainless steel, and earthenware) had a nominal working volume of 2 hL, while bottles were 750 mL. Each storage condition was prepared in three independent experimental replicates (n = 3), which were maintained and sampled separately throughout the experiment. (Figure 1). Earthenware sampling was available up to 90 days (T0–T3), whereas the other conditions were monitored up to 150 days (T0–T5).

Consequently, comparisons involving earthenware were restricted to the available 0–90-day interval, and this condition was not interpreted for late-stage processes occurring beyond day 90.

2.2. Design and Fabrication of Corian® Tanks

Corian® tanks were custom-designed to match the working volume and surface-to-volume ratio of the reference stainless steel pilot tanks, minimizing confounding effects due to geometry. Tank fabrication was performed by Niccolini Giorgio (Ancona, Italy). Corian® sheets (12 mm thickness) were CNC-cut to obtain the base, lid, and side panels, including openings for sampling tap, drain valve, and airlock. Components were assembled using a dedicated adhesive under clamping pressure (two mirrored half-shells were constructed

and subsequently joined). Internal joints were sanded progressively from P80 to P500 grit to remove adhesive residues and obtain a smooth, non-retentive surface comparable to electropolished stainless steel. Tanks were equipped with sealed or floating lids, airlock, sampling tap, and drain. No thermal insulation was applied to either Corian® or stainless steel tanks.

Figure 1. Schematic representation of the experimental design showing the three bulk storage conditions (Corian® tanks, stainless steel tanks, raw earthenware amphorae, glass bottles). Bulk vessels had a nominal working volume of 2 hL, whereas bottles were 0.75 L. Sampling times covered T0–T5 for Corian®, stainless steel, and bottles; earthenware was available up to T3 (90 days). The schematic was graphically redrawn from the experimental setup to include all storage conditions investigated in the study.

2.3. Environmental and Temperature Monitoring

Ambient cellar temperature was monitored near each container type. To assess thermal inertia of the wine mass, submerged data loggers (HOBO TidbiT MX Temperature 5000, Onset Computer Corp., Bourne, MA, USA) were placed inside each bulk container and recorded wine temperature at 6 h intervals throughout the aging period. For bottles, loggers were positioned in the immediate proximity of the bottle storage area to capture the local thermal dynamics experienced by the finite-volume system.

2.4. Sampling Strategy and On-Site Physicochemical Measurements

To minimize oxygen ingress during sampling, a closed-loop recirculation system was implemented for bulk containers (Figure 2). The use of a rotary piston pump (Fluid-o-Tech Srl, Corsico, Milan, Italy) was deliberately selected to ensure controlled and low-shear circulation conditions.

All fluidic connections were assembled using hermetically sealed fittings, and food-grade tubing with low oxygen permeability was used throughout the recirculation loop. Prior to each measurement, the circuit was completely filled with wine to eliminate residual headspace and minimize gas exchange with the external environment.

The closed-loop configuration was designed to minimize oxygen exposure during measurement by avoiding direct contact between the circulating wine and ambient air. While a dedicated validation experiment was not performed in the present study, previous work has shown that compositional effects of short pumping operations are mainly associated with oxygen exposure and mechanical energy input; under sealed, short-duration

recirculation, these effects are expected to be limited relative to the aging trends investigated here [14,15].

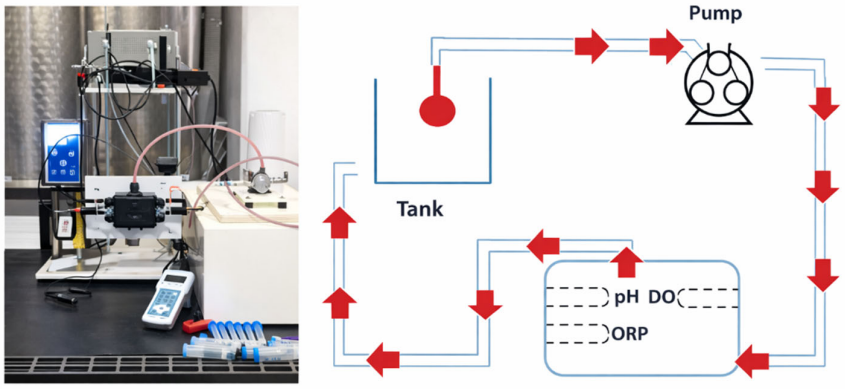

Figure 2. Closed-loop measurement system for non-invasive monitoring of wine physicochemical parameters. Wine was circulated from the container through food-grade tubing by a 24 V rotary piston pump into a hermetically sealed flow-through measurement cell housing, and then returned to the container. The closed-loop configuration minimized oxygen ingress and ensured controlled hydrodynamic conditions. Measurements were performed after signal stabilization (15 min), with sampling at mid-depth of the wine column to limit stratification effects. The red arrows indicate the wine flow direction within the closed-loop circuit. The image was graphically refined for clarity without altering the experimental configuration.

In the present study, the recirculation system was therefore conceived as a measurement interface rather than as a perturbative operation, allowing reliable monitoring of redox and oxygen-related parameters without altering the underlying chemical trajectories. Hence, at each monthly sampling point, wine was circulated through a sealed flow-through measurement cell and returned to the container headspace region. Dissolved oxygen (DO) was measured using an optical sensor (InPro 6850i, Mettler-Toledo, Milan, Italy) connected to an M700X transmitter (Mettler-Toledo, Milan, Italy). Oxidation–reduction potential (ORP) and pH were measured using KP90 and KP20 probes (Delta Ohm, Padua, Italy) connected to a portable multiparametric data logger (HD 98569, Delta Ohm, Padua, Italy). Measurements were performed by sampling at approximately mid-depth of the wine column. This position was selected to minimize potential stratification effects, while the short-duration recirculation step was intended to promote representative bulk measurements within each storage vessel.

Measurements were acquired only after complete stabilization of all electrochemical signals (typically ≈15 min under the operating conditions adopted), consistent with sensor manufacturer specifications and previous applications of electrochemical probes in oxidation-sensitive liquid food matrices.

For bottled wines, destructive sampling was adopted (distinct bottles opened and analyzed at each time point). In fact, unlike bulk systems, bottle measurements necessarily required opening the sealed container prior to analysis. Therefore, bottle measurements should be interpreted as endpoint descriptors of the preceding sealed storage condition rather than as strictly equivalent in situ measurements, and this limitation should be considered when comparing bulk and bottle redox dynamics.

2.5. Chemical and Colorimetric Analyses

At each sampling time, aliquots were collected for laboratory analyses. Standard oenological parameters—including free and total sulfur dioxide, total anthocyanins (A_{tot}), polymerized pigments (PPs), total polyphenols, and tannins—were determined using a CDR WineLab® photometric analyzer (CDR Srl, Ginestra Fiorentina, Florence, Italy) with

pre-calibrated reagent kits. Color density and hue were determined spectrophotometrically, as well as abosorbance indices A420, A520, and A620.

2.6. Statistical Analysis and Kinetic Modeling

Prior to statistical analysis, datasets were screened for completeness, internal consistency, and outliers. Temperature was excluded from multivariate analysis to avoid dominance effects unrelated to wine chemical composition. Quantitative variables were mean-centered and variance-scaled before multivariate treatment. Principal component analysis (PCA) was applied as an exploratory tool to investigate global data structure and visualize similarities/divergences among storage conditions without imposing a priori classification. Loadings were used to support interpretation of the variables associated with major score-space directions.

Kinetic modeling was conducted on time-resolved concentration data for selected physicochemical parameters.

Model formulations were selected a priori on the basis of established kinetic descriptions reported in wine aging studies and the expected physicochemical behavior of each variable. Model adequacy was subsequently evaluated through coefficients of determination (R^2) and residual inspection, with the objective of obtaining interpretable comparative descriptors rather than selecting an optimal predictive model among competing formulations.

DO was modeled using a temperature-adjusted pseudo-first-order formulation (Equation (1)). First-order kinetics for free sulfur dioxide (FSO_2) consumption were described according to Equation (2). Preliminary inspection of the experimental time-series revealed deviations from a strictly monotonic decay at extended storage times. Consequently, a piecewise kinetic approach was adopted, and first-order regressions were restricted to the early storage phase (0–90 days), during which net SO_2 consumption was dominant.

The 90-day threshold was selected because it corresponded to the onset of systematic deviations from monotonic behavior observed across multiple redox-related variables, particularly FSO_2 and ORP, and was therefore used as a pragmatic segmentation point rather than a statistically optimized breakpoint.

Equation (2) was fitted separately to each experimental replicate (R1–R3), and kinetic parameters are reported as mean ± standard deviation (n = 3). PP formation was modeled assuming zero-order kinetics according to Equation (3). The same zero-order formulation was also applied to absorbance at 420 nm (ABS420) as an optical descriptor of color evolution. Also in this case, Equation (3) was fitted separately to each experimental replicate (R1–R3), and kinetic parameters are reported as mean ± standard deviation (n = 3); R^2 values correspond to the mean coefficient of determination obtained from replicate-specific regressions. ORP evolution in bulk inert systems was modeled using a piecewise linear regression approach separating an initial reduction phase (0–90 days) from a rebound phase (90–150 d) (Equation (4)), i.e., the same approach applied for free SO_2. Due to high variability and limited explanatory power, ORP data from bottled wines were evaluated descriptively.

Model formulations were selected a priori on the basis of established kinetic descriptions in wine aging studies and the expected physicochemical behavior of each variable. Model adequacy was then evaluated through coefficients of determination and residual inspection, with the aim of obtaining interpretable comparative descriptors rather than selecting an optimal predictive model among competing formulations.

Details about the above models and equations follow here.

DO was modeled using a temperature-adjusted pseudo-first-order formulation:

$$\ln[\mathrm{DO}] = \ln[\mathrm{DO}]_0 - k_{\mathrm{obs}}t + \gamma T \quad (1)$$

where k_{obs} (day^{-1}) is the apparent oxygen consumption parameter and γ ($^{\circ}\mathrm{C}^{-1}$) accounts for temperature effects, as previously proposed for describing oxygen kinetics in wine systems under variable thermal conditions [8,17].

FSO_2 depletion was described using an apparent first-order model and piecewise linear approach:

$$\ln\left(\frac{C_{\mathrm{FSO_2\_}t}}{C_{\mathrm{FSO_2\_0}}}\right) = \begin{cases} -k_1 t, & \text{for} \leq t \leq t_c \\ \text{not fitted} & \text{for } t > t_c \end{cases} \quad (2)$$

where $C_{\mathrm{FSO2\_}t}$ is the concentration of free SO_2 at time t, $C_{\mathrm{FSO2\_0}}$ is the initial free SO_2 concentration at t = 0, and k_1 is the apparent first-order rate constant during the early storage phase. The corresponding half-time was calculated as $t_{1/2} = \ln(2)/k_1$. The parameter t_c = 90 days represents the time limit beyond which the model was not applied. As already mentioned, preliminary inspection of the experimental time-series revealed deviations from a strictly monotonic decay of FSO_2 at extended storage times. Therefore, Equation (2) was applied using a piecewise approach, restricting the regression to the early storage interval (0–90 days), when net SO_2 consumption was dominant. First-order kinetics for free SO_2 consumption are widely reported in the literature and reflect its role as a primary redox buffer during wine aging [9,22].

PA accumulation was described using a zero-order model:

$$C_{\mathrm{PA\_}t} = C_{\mathrm{PA\_0}} + k_0 t \quad (3)$$

where $C_{\mathrm{PA\_}t}$ is the concentration of PA at time t; $C_{\mathrm{PA\_0}}$ was the initial concentration of PA at t = 0, and k_0 represents the average rate of pigment formation. Zero-order behavior is consistent with polymerization processes limited by the availability of reactive intermediates rather than by precursor concentration [3,6].

Because ORP evolution in bulk inert systems showed non-monotonic behavior, it was modeled using a piecewise linear approach, conceptually similar to that applied to FSO_2 but based on linear slopes rather than first-order depletion constants:

$$\mathrm{ORP}_t = \begin{cases} f(x) = \begin{cases} \mathrm{ORP}_0 + k_1 t, & 0 \leq t \leq 90 \\ \mathrm{ORP}_{90} + k_2(t-90), & t \geq 90 \end{cases} \end{cases} \quad (4)$$

where ORP_t was the oxidation–reduction potential at time t (mV); ORP_0 was the initial ORP value at t = 0; ORP_{90} was the value at the transition time (90 days); k_1 was the linear slope of ORP variation during the initial reduction phase (0–90 days) (mV day^{-1}); k_2 was the linear slope of ORP variation during the post-90-day phase (90–150 days), describing the redox rebound (mV day^{-1}). The use of ORP as an integrative redox descriptor linking oxygen availability, sulfur dioxide consumption, and phenolic evolution is well established in wine aging studies [8,25].

The statistical treatment adopted in this study was descriptive and comparative rather than inferential. Accordingly, the analysis focused on replicate-level kinetic descriptors and goodness-of-fit diagnostics, with the aim of comparing boundary-condition-dependent reaction behavior rather than testing formal statistical differences among storage systems.

Regressions were performed on individual experimental replicates using ordinary least squares. Reported parameters represent mean values ± standard deviation, calculated across replicates where applicable. Model adequacy was evaluated using coefficients of

determination (R^2) and visual inspection of residuals. Statistical analyses and data visualization were conducted in Python v3.11 (Python Software Foundation, Wilmington, DE, USA) within the JupyterLab environment. PCA and regression modeling were performed using standard scientific libraries, including NumPy, pandas, scikit-learn, and statsmodels, along with JASP software Version: JASP 0.95.4 (University of Amsterdam, Amsterdam, The Netherlands). The latter has been used to generate Figure 3.

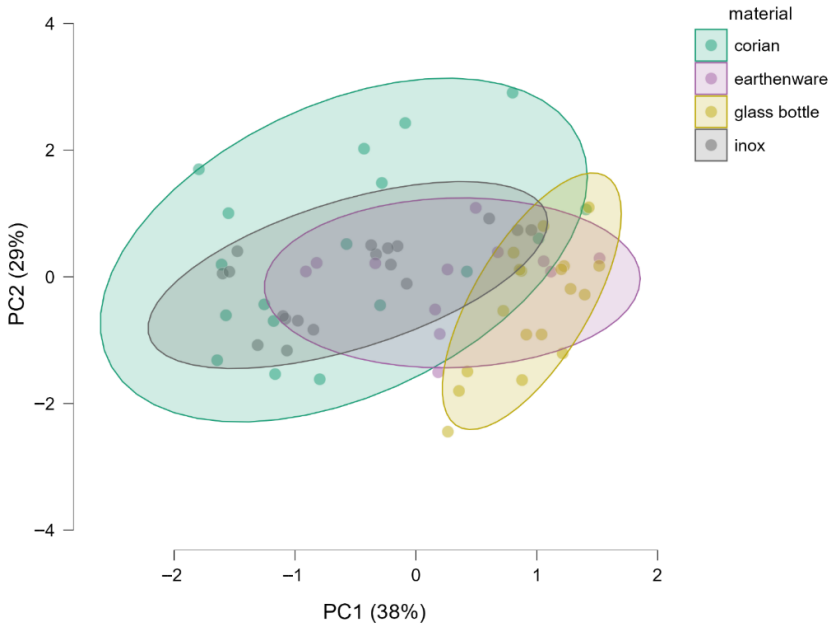

Figure 3. Principal component analysis (PCA) score plot based on dissolved oxygen (DO), free sulfur dioxide (FSO_2), polymerized pigments (PP), and oxidation–reduction potential (ORP). Data were auto-scaled prior to analysis. PC1 and PC2 explained 38% and 29% of the total variance, respectively. Points represent individual samples colored by storage condition. Ellipses represent 95% confidence regions based on the dispersion of samples within each storage condition in the PC1–PC2 space.

3. Results and Discussion

To provide an integrated overview of the multivariate organization of the dataset prior to kinetic modeling, PCA was initially applied to the full set of measured chemical and colorimetric variables, excluding temperature. Data were auto-scaled to ensure equal contribution of all parameters. As previously reported for complex wine aging systems, strong covariance among phenolic, chromatic, and sulfur dioxide-related variables can obscure the identification of dominant drivers of chemical evolution in multivariate space [3,16]. Accordingly, the PCA score plot based on the complete variable set revealed only partial separation of samples according to storage conditions, with substantial overlap among clusters. To better resolve differences among storage environments and to focus on variables directly linked to redox and oxidative processes, PCA was subsequently performed considering only parameters that exhibited consistent and mechanistically interpretable kinetic behavior, namely DO, FSO_2, PP, and ORP This reduced-variable PCA resulted in a markedly improved clustering of storage conditions. PC1 and PC2 explained 38% and 29% of the total variance, respectively. Because PCA was applied here as an exploratory multivariate visualization tool rather than as an inferential clustering method, the interpretation focuses on score dispersion and covariance structure rather than formal cluster significance testing (Figure 3).

Inert bulk systems (Corian® and stainless steel) formed compact and partially overlapping clusters, indicating similar redox-controlled trajectories, whereas earthenware samples

were clearly separated, consistent with boundary-condition effects associated with porous storage. Bottle-aged samples displayed higher dispersion but occupied a distinct region of the multivariate space, reflecting a less constrained and more heterogeneous oxidative evolution. This PCA supports the interpretation that storage-driven chemical evolution is governed by a limited set of redox-related descriptors rather than by uniform contributions from all measured parameters, in agreement with previous mechanistic frameworks proposed for wine aging under controlled oxidative conditions [9,22]. Absorbance at 420 nm (ABS420) was not included in the reduced-variable PCA due to its strong covariance with PP and other chromatic descriptors. At the same time, being a widely used indicator of oxidative color development, it was therefore later analyzed separately as a univariate kinetic indicator of color evolution.

Although temperature was excluded from PCA, its temporal dynamics differed markedly among storage systems and contributed to defining the boundary conditions of the aging reactors. Temperature recordings (summarized in Table 1) indicated that bulk systems exhibited limited thermal oscillations over the aging period, consistent with high thermal inertia of the wine mass. In contrast, bottles showed substantially larger and more frequent thermal fluctuations, reflecting rapid heat exchange associated with reduced volume and a higher surface-to-volume ratio. Quantitatively, bottles displayed a threefold higher mean daily temperature range (ΔT) than bulk inert containers (Table 1), supporting the interpretation of bottle aging as a thermally responsive micro-reactor. Similar reactor-based interpretations of temperature control and thermal buffering effects have been proposed in enological systems, highlighting the role of vessel-scale heat exchange in modulating reaction kinetics [26].

Table 1. Thermal variability of wine storage systems during the aging period.

Storage System	Mean Temperature (°C)	Mean Daily ΔT (°C)	Max Observed ΔT (°C)	Thermal Behavior
Corian® (bulk inert)	19.4 ± 1.8	2.1 ± 0.3	3.0	High thermal inertia
Stainless steel (bulk inert)	19.5 ± 1.9	2.3 ± 0.4	3.2	High thermal inertia
Earthenware (bulk porous)	19.6 ± 2.1	2.8 ± 0.5	3.8	Moderate thermal inertia
Glass bottle (0.75 L)	19.7 ± 2.6	6.5 ± 0.8	8.1	Low thermal inertia

Note: Values are reported as mean ± standard deviation across replicates where applicable. ΔT indicates the daily temperature range. The markedly higher temperature variability observed in bottles reflects reduced thermal inertia associated with the finite-volume configuration.

These boundary-condition differences provide a mechanistic basis for divergent kinetic behavior. Because the observed temperature profiles emerged from naturally occurring storage-specific fluctuations rather than from experimentally imposed isothermal treatments, temperature was not treated as an independent kinetic variable suitable for Arrhenius-type modeling. Instead, thermal behavior was interpreted here as an emergent boundary-condition descriptor contributing to the divergence between bulk and bottle aging regimes. In particular, thermal variability should be interpreted as a co-driving boundary condition, together with oxygen availability and storage geometry, rather than as a secondary environmental factor. Frequent temperature fluctuations may modulate effective reaction rates through temperature-dependent changes in solubility, diffusion, and chemical reactivity, even when oxygen transfer remains limited.

Following the exploratory PCA and temperature characterization, the experimental results were interpreted within a reaction-kinetics framework in which each wine–container system was considered as a reactor defined by vessel permeability, gas transmission characteristics, storage volume, and thermal exchange properties [4]. Kinetic parameters were

therefore used as comparative descriptors of storage-specific boundary conditions rather than as universal intrinsic reaction constants [17].

Apparent oxygen parameters estimated with Equation (1) are reported in Table 2. In inert bulk systems, the estimated k_{obs} values were on the order of 10^{-2} day^{-1}, with negative γ terms indicating an inverse temperature association in the fitted relationship, consistent with the opposing effects of temperature on oxygen solubility and reaction kinetics [8,17].

Table 2. Apparent oxygen consumption parameters estimated using Equation (1) (temperature-adjusted pseudo-first-order model).

Storage System	k_{obs} (day^{-1}) *	γ (°C^{-1})	Mean R^2	n
Corian®	0.0171 ± 0.0021	−0.0827 ± 0.0020	0.93	3
Stainless steel	0.0120 ± 0.0010	−0.0548 ± 0.0012	0.98	3
Raw earthenware	0.0113 ± 0.0050	0.0166 ± 0.0045	0.91	3
Glass bottle	0.0031 ± 0.0005	−0.0058 ± 0.0004	0.95	3

* k_{obs} is an apparent oxygen parameter integrating intrinsic wine oxygen demand and boundary-condition effects; γ accounts for the temperature term in the fitted relationship. Values are reported as mean ± standard deviation across replicates (n = 3). Mean R^2 refers to replicate-level regressions.

In permeable systems such as earthenware, Equation (1) must be interpreted cautiously because continuous oxygen ingress violates the closed-reactor assumption embedded in a consumption-only formulation [11,12]. Therefore, the earthenware k_{obs} value is reported only as an apparent boundary-condition-dependent descriptor and is not directly compared with inert bulk or bottle systems as an intrinsic oxygen consumption rate.

Bottle k_{obs} values were lower (Table 2), consistent with a boundary condition characterized by low oxygen transfer through the closure [18–20]; nevertheless, as shown by other kinetic descriptors below, bottle aging did not behave as a simple slowed continuation of bulk aging.

As described above, free SO_2 evolution deviated from a strictly monotonic decay across all materials, particularly at extended storage times. Consequently, first-order kinetics were applied exclusively to the early storage phase (0–90 days), during which net SO_2 consumption was dominant. The resulting rate constants reported in Table 3 therefore represent apparent first-order descriptors of early-stage SO_2 depletion. When considering the 0–90-day interval, inert bulk systems exhibited the highest apparent depletion rate constants. Stainless steel showed the fastest early-stage free SO_2 consumption ($k_1 = 9.4 \times 10^{-3}$ day^{-1}), followed by Corian® ($k_1 = 7.1 \times 10^{-3}$ day^{-1}). Earthenware displayed intermediate behavior ($k_1 = 5.8 \times 10^{-3}$ day^{-1}), whereas bottle-aged wines exhibited the lowest apparent rate constant in this phase ($k_1 = 3.2 \times 10^{-3}$ day^{-1}), corresponding to the longest half-life among the investigated systems. These differences are consistent with the combined effects of oxygen availability, redox buffering capacity, and storage geometry on sulfur dioxide consumption reported in previous kinetic and mechanistic studies [9,16,17]. Beyond the early storage phase, FSO_2 evolution increasingly departed from monotonic behavior, reflecting the establishment of redox-buffered conditions. Accordingly, the apparent rate constants reported in Table 3 should be interpreted as comparative descriptors of early-stage SO_2 consumption rather than as global kinetic parameters describing the entire aging period, in agreement with previous observations in complex wine aging environments [1,22].

Because A_{tot} did not always support robust full-curve fitting, an endpoint-based apparent first-order descriptor was computed (Table 4), an approach commonly adopted when phenolic evolution deviates from strict monotonic behavior during aging [3,6]. Bottle wines showed an apparent $k_{Atot,\,endpoint} = 0.93 \times 10^{-3}$ day^{-1}, while stainless steel exhibited 1.49×10^{-3} day^{-1} and Corian® 0.49×10^{-3} day^{-1}. Earthenware displayed a negative end-

point descriptor (-2.48×10^{-3} day^{-1}), indicating a net increase in A_{tot} over the available 0–90 days window in this dataset; this confirms that in porous storage the anthocyanin trajectory may not be representable as a simple monotonic decay and supports the decision to treat A_{tot} with a pragmatic net descriptor rather than a single global kinetic law, in agreement with previous observations on oxygen-driven pigment formation in porous containers [5,7,13].

Table 3. Apparent first-order rate constants (k1) for free SO_2 consumption during early storage (0–90 days).

Material	k_1 ($\times 10^{-3}$ day^{-1}) *	R^2	n
Corian	7.1 ± 1.9	0.78 ± 0.06	3
Inox	9.4 ± 2.2	0.81 ± 0.04	3
Earthenware	5.8 ± 2.5	0.69 ± 0.10	3
Glass bottle	3.2 ± 1.8	0.62 ± 0.12	3

* Rate constants were obtained by fitting Equation (2) to the 0–90-day intervals only. Regressions were performed separately for each experimental replicate (R1–R3), and kinetic parameters are reported as mean ± standard deviation (n = 3).

Table 4. Endpoint-based apparent first-order descriptor for total anthocyanins (A_{tot}).

Storage System	$k_{Atot,\ endpoint}$ ($\times 10^{-3}$ Day^{-1}) *	SD	n
Corian®	0.49	0.15	3
Stainless steel	1.49	0.34	3
Raw earthenware	−2.48	0.11	3
Glass bottle	0.93	0.49	3

* The apparent rate constant was computed as $k = -\ln(C_{end}/C_0)/t_{end}$ for each replicate and reported as mean ± standard deviation (n = 3). This descriptor integrates the net anthocyanin change over time when full-curve fitting is not robust due to non-monotonic behavior.

PPs were described using a zero-order model (Equation (3); Table 5), consistent with kinetic formulations previously applied to pigment polymerization under oxygen-limited or intermediate-controlled conditions [6,10]. Based on replicate-specific regressions, Corian® and glass bottle systems exhibited comparable apparent formation rate constants (0.094 and 0.084 PA units day^{-1}, respectively), whereas stainless steel showed a lower average rate (0.047 PA units day^{-1}), indicating a slower accumulation of PP under more inert bulk storage conditions.

Table 5. Zero-order formation parameters for polymerized pigments (PP) (Equation (3)).

Material	k_0,PA (PA units day^{-1}) *	R^2, PA (Mean) *	k_0,ABS420 (ABS units day^{-1}) *	R^2, ABS420 (Mean) *	n
Corian®	0.0943 ± 0.0184	0.770	−0.001754 ± 0.000650	0.375	3
Stainless steel (Inox)	0.0472 ± 0.0161	0.610	+0.000517 ± 0.000438	0.126	3
Glass bottle	0.0837 ± 0.0259	0.602	−0.000563 ± 0.000228	0.095	3

* Rate constants were obtained from zero-order fits (Equation (3)) applied separately to each replicate (R1–R3). Reported values represent mean ± standard deviation (n = 3). R^2 values correspond to the mean coefficient of determination obtained from replicate-specific regressions. Earthenware was excluded from the zero-order analysis due to sampling limited to 90 days.

Absorbance at 420 nm (ABS420), analyzed in parallel as an optical descriptor of color evolution, displayed markedly lower apparent zero-order rate constants and higher variability across storage conditions (Table 5). This behavior reflects the integrative and indirect nature of ABS420, which captures the cumulative optical outcome of multiple

underlying reactions rather than a single compositional process. Accordingly, while PA accumulation was reasonably approximated by linear trends over time at the replicate level, ABS420 evolution showed weaker linearity over the full storage interval, consistent with previous reports of non-linear chromatic evolution during wine aging [3,17].

ORP was used as an integrative descriptor of the redox environment, complementing DO and FSO_2 dynamics. In inert bulk systems, ORP decreased rapidly from positive values at T0 to strongly negative values within the first 90 days, indicating the establishment of a reducing regime [8,9]. Over the full 0–150 day period, ORP evolution in bulk inert storage was not strictly monotonic, showing a partial rebound after day 90; accordingly, a piecewise formulation (Equation (4)) was applied for these conditions, and the resulting parameters are summarized in Table 6, consistent with previous reports of non-linear redox evolution during wine aging [25,27].

Table 6. Piecewise kinetic parameters for ORP evolution (Equation (4)).

Material	Segment (days)	n	k (mV·day^{-1}) *	R^2 *
Corian®	0–90	12	−1.064	0.920
Stainless steel	0–90	12	−0.931	0.813
Glass bottle	0–90	12	−0.212	0.542
Earthenware	0–90	12	−0.566	0.647
Corian®	90–150	9	+0.422	0.325
Stainless steel	90–150	9	+0.387	0.305
Glass bottle	90–150	9	+0.009	~0.000
Earthenware	90–150	—	—	—

* Slope units are mV·day^{-1}. R^2 refers to the linear fit within each time segment. Positive k_2 indicates a partial shift back toward more oxidizing potentials after day 90. Earthenware was sampled only up to 90 days; therefore, a post-90 days segment cannot be estimated.

In bottles, ORP exhibited higher variability, including transient oxidizing excursions. Although piecewise fits are reported for completeness in Table 6, the very low explanatory power observed for the late bottle segment indicates that ORP behavior in bottles should be interpreted descriptively rather than as a robust kinetic outcome, reflecting the higher sensitivity of bottled wine redox status to closure-mediated oxygen transfer, stopper-to-stopper variability, finite-volume effects, and episodic redox shifts [18,19].

Because earthenware data were available only up to day 90, this condition was not included in the interpretation of the post-90-day rebound phase.

From a mechanistic perspective, ORP integrates oxygen availability, sulfur dioxide buffering, and phenolic reactivity. In bulk inert storage, the sustained decrease in ORP is consistent with oxygen depletion combined with SO_2-mediated redox buffering, which can limit the propagation of oxidative phenolic cascades [3,9]. In the finite-volume regime, increased ORP variability suggests reduced buffering stability and enhanced sensitivity to episodic redox shifts, supporting the broader "divergent kinetic" framework and the distinct post-bottling reaction pathways described for bottled wines [21,22].

4. Conclusions

This study applied an integrated multivariate and kinetic framework to compare wine evolution under bulk storage and bottle aging conditions. PCA revealed compact and overlapping trajectories for inert bulk systems, whereas bottle-aged samples showed greater dispersion, indicating a less constrained chemical evolution. Monitoring of thermal bound-

ary conditions further demonstrated that bottles experienced markedly reduced thermal inertia, with substantially larger daily temperature fluctuations than bulk containers.

Kinetic descriptors highlighted that storage scale and boundary conditions influence wine evolution beyond simple differences in reaction rate. DO parameters required cautious interpretation in permeable systems, FSO_2 descriptors were meaningful only during early storage, and ORP showed that bulk inert systems developed a more stable reducing regime, whereas bottles displayed greater redox variability. Anthocyanins were better summarized using endpoint descriptors, while polymerized pigments followed an approximately zero-order accumulation in the modeled systems.

Although the present work was conducted on a single wine matrix under controlled experimental conditions and without a strict anaerobic control, the results support the concept that bottle aging may represent a boundary-condition-dependent kinetic regime distinct from bulk storage. The observed kinetic patterns should therefore be interpreted within the specific experimental framework investigated here rather than as universally transferable principles. From an applied perspective, bottling timing and post-bottling storage should be managed as a distinct technological phase requiring dedicated strategies that account for finite-volume thermal responsiveness, oxygen exchange, and enhanced redox variability.

Future studies should extend this framework to additional cultivars, closure systems, oxygen-management scenarios, and controlled anaerobic reference conditions in order to further test the generality of the proposed boundary-condition-dependent kinetic approach.

Author Contributions: Conceptualization, P.M. and A.P.; methodology, P.M.; software, P.M.; validation, P.M. and G.A.; formal analysis, P.M. and G.A.; investigation, P.M., A.S., F.C. and G.A.; resources, P.M. and A.P.; data curation, P.M., F.C. and G.A.; writing—original draft preparation, P.M.; writing—review and editing, P.M., A.S. and F.C.; visualization, P.M. and F.C.; supervision, P.M. and A.P. All authors have read and agreed to the published version of the manuscript.

Funding: This research received no external funding.

Institutional Review Board Statement: Not applicable.

Informed Consent Statement: Not applicable.

Data Availability Statement: The original contributions presented in this study are included in the article. Further inquiries can be directed to the corresponding author.

Acknowledgments: The authors would like to thank Fattoria di Petrognano for hosting the experimental trials, in particular to Monica Rossetti and all the winery's staff for their technical support. Thanks also to Giorgio Niccolini's Company for providing the Corian® materials and Damiano Niccolini for his help during trials and data processing. The authors used ChatGPT 5.2/January 2026 for English language refinement and graphical polishing of Figures 1 and 2. The tool was not used to generate or modify experimental data. The authors reviewed and edited all outputs and take full responsibility for the content of this publication.

Conflicts of Interest: The authors declare no conflicts of interest.

Abbreviations

The following abbreviations are used in this manuscript:

DO	Dissolved oxygen
ORP	Oxidation–reduction potential
A_{tot}	Total anthocyanins
PP	Polymerized pigments
PCA	Principal component analysis
FSO_2	Free sulfur dioxide

References

1. Ribéreau-Gayon, P.; Glories, Y.; Maujean, A.; Dubourdieu, D. *Handbook of Enology, Vol. 2: The Chemistry of Wine—Stabilization and Treatments*, 3rd ed.; John Wiley & Sons Ltd.: Chichester, UK, 2021.
2. Waterhouse, A.L.; Sacks, G.L.; Jeffery, D.W. *Understanding Wine Chemistry*, 2nd ed.; John Wiley & Sons Ltd.: Chichester, UK, 2016.
3. Cheynier, V.; Dueñas-Paton, M.; Salas, E.; Maury, C.; Souquet, J.-M.; Sarni-Manchado, P.; Fulcrand, H. Structure and properties of wine pigments and tannins. *Am. J. Enol. Vitic.* **2006**, *57*, 298–305. [CrossRef]
4. Del Alamo-Sanza, M.; Nevares, I. Oak wine barrel as an active vessel: A critical review of past and current knowledge. *Crit. Rev. Food Sci. Nutr.* **2018**, *58*, 2711–2726. [CrossRef] [PubMed]
5. Fulcrand, H.; Cameira dos Santos, P.-J.; Sarni-Manchado, P.; Cheynier, V.; Favre-Bonvin, J. Structure of new anthocyanin-derived wine pigments. *J. Chem. Soc. Perkin Trans. 1* **1996**, *7*, 735–739. [CrossRef]
6. Gambuti, A.; Picariello, L.; Rinaldi, A.; Moio, L. Evolution of Sangiovese wines with varied tannin and anthocyanin ratios during oxidative aging. *Front. Chem.* **2018**, *6*, 63. [CrossRef]
7. Garrido-Bañuelos, G.; Buica, A.; Sharp, E.; de Villiers, A.; Du Toit, W.J. The impact of different tannin-to-anthocyanin ratios and of oxygen on phenolic polymerisation in a wine-like solution. *S. Afr. J. Enol. Vitic.* **2019**, *40*, 192–210. [CrossRef]
8. Danilewicz, J.C. Review of reaction mechanisms of oxygen and proposed intermediate reduction products in wine: Central role of iron and copper. *Am. J. Enol. Vitic.* **2003**, *54*, 73–85. [CrossRef]
9. Danilewicz, J.C. Interaction of sulfur dioxide, polyphenols, and oxygen in a wine-model system: Central role of iron and copper. *Am. J. Enol. Vitic.* **2007**, *58*, 53–60. [CrossRef]
10. Picariello, L.; Gambuti, A.; Petracca, F.; Rinaldi, A.; Moio, L. Enological tannins affect acetaldehyde evolution, colour stability and tannin reactivity during forced oxidation of red wine. *Int. J. Food Sci. Technol.* **2018**, *53*, 228–236. [CrossRef]
11. Del Alamo-Sanza, M.; Nevares, I. Recent advances in the evaluation of the oxygen transfer rate in oak barrels. *J. Agric. Food Chem.* **2014**, *62*, 8892–8899. [CrossRef]
12. Junqua, R.; Zeng, L.; Pons, A. Oxygen gas transfer through oak barrels: A macroscopic approach. *OENO One* **2021**, *55*, 53–65. [CrossRef]
13. Nevares, I.; Del Alamo-Sanza, M. Characterization of the oxygen transmission rate of new-ancient natural materials for wine maturation containers. *Foods* **2021**, *10*, 140. [CrossRef]
14. Masella, P.; Angeloni, G.; Guerrini, L.; Spadi, A.; Maioli, F.; Calamai, L.; Parenti, A. A deeper understanding of the qualitative consequences of food pumping: A case study of wine. *Food Bioprod. Process.* **2022**, *131*, 13–21. [CrossRef]
15. Guerrini, L.; Breschi, C.; Zanoni, B.; Calamai, L.; Angeloni, G.; Masella, P.; Parenti, A. Filtration Scheduling: Quality Changes in Freshly Produced Virgin Olive Oil. *Foods* **2020**, *9*, 1067. [CrossRef]
16. Petrozziello, M.; Torchio, F.; Piano, F.; Giacosa, S.; Ugliano, M.; Bosso, A.; Rolle, L. Impact of increasing levels of oxygen consumption on the evolution of color, phenolic, and volatile compounds of Nebbiolo wines. *Front. Chem.* **2018**, *6*, 137. [CrossRef] [PubMed]
17. Pérez-Magariño, S.; Martínez-Gil, A.M.; Bueno-Herrera, M.; Nevares, I.; Del Alamo-Sanza, M. Kinetics of oxygen consumption, a key factor in the changes of young wine composition. *LWT–Food Sci. Technol.* **2023**, *182*, 114786. [CrossRef]
18. Godden, P. Summary of AWRI closure trials and understanding closure performance. *AWRI Tech. Rev.* **2020**, *248*, 7–17.
19. Lopes, P.; Saucier, C.; Teissedre, P.-L.; Glories, Y. Impact of storage position on oxygen ingress through different closures into wine bottles. *J. Agric. Food Chem.* **2006**, *54*, 6741–6746. [CrossRef]
20. Lopes, P.; Saucier, C.; Teissedre, P.-L.; Glories, Y. Main routes of oxygen ingress through different closures into wine bottles. *J. Agric. Food Chem.* **2007**, *55*, 5167–5170. [CrossRef]
21. Boulet, J.-C.; Vernhet, A.; Poncet-Legrand, C.; Cheynier, V.; Doco, T. Exploring the role of grape cell wall and yeast polysaccharides in extraction and stabilisation of anthocyanins and tannins in red wines. *OENO One* **2024**, *58*, 1. [CrossRef]
22. Ugliano, M. Oxygen contribution to wine aroma evolution during bottle aging. *J. Agric. Food Chem.* **2013**, *61*, 6125–6136. [CrossRef]
23. Carrasco-Quiroz, M.; Martínez-Gil, A.M.; Nevares, I.; Del Alamo-Sanza, M. New system for simultaneous measurement of oxygen consumption and changes in the wine color. *Molecules* **2024**, *29*, 231. [CrossRef]
24. Cebrián-Tarancón, C.; Sánchez-Gómez, R.; Martínez-Gil, A.M.; Del Alamo-Sanza, M.; Nevares, I.; Salinas, M.R. Evolution during bottle ageing of wines macerated with toasted vine-shoots and micro-oxygenation. *Biomolecules* **2024**, *14*, 1372. [CrossRef]
25. Guerrini, L.; Maioli, F.; Picchi, M.; Zanoni, B.; Parenti, A.; Canuti, V. Kinetic modeling of a Sangiovese wine's chemical and physical parameters during one-year aging in different tank materials. *Eur. Food Res. Technol.* **2022**, *248*, 1525–1539. [CrossRef]

26. Masella, P.; Angeloni, G.; Corti, F.; Spadi, A.; Garbati Pegna, F.; Guerrini, L.; Parenti, A. Innovative thermal control of fermentations through the use of phase change materials: A focus on wine fermentation. *Appl. Food Res.* **2025**, *5*, 100688. [CrossRef]
27. Vivas, N.; Zamora, F.; Glories, Y. Etude des phénomènes d'oxydoréduction dans les vins. Mise au point d'une méthode rapide de mesure du potentiel d'oxydoréduction. *OENO One* **1992**, *26*, 271–285. [CrossRef]